Available online at www.sciencedirect.com
ScienceDirect
Antiviral Research 72 (2006) 207–215
Antiviral Research
www.elsevier.com/locate/antiviral

Solution conformation of an immunodominant epitope in the hepatitis B virus preS2 surface antigen

Seung-Wook Chi [a], Do-Hyoung Kim [a], Jae-Sung Kim [a], Myung Kyu Lee [b], Kyou-Hoon Han [a,*]

[a] *Molecular Cancer Research Center, Division of Molecular Therapeutics, Korea Research Institute of Bioscience and Biotechnology, Yusong P.O. Box 115, Daejon, Korea*

[b] *Systemic Proteomics Research Center, Korea Research Institute of Bioscience and Biotechnology, Yusong P.O. Box 115, Daejon, Korea*

Received 14 April 2006; accepted 13 June 2006

Abstract

We have determined the solution conformation of the major B cell epitope (residues 123–145, adrl23 hereafter) in the preS2 region of hepatitis B virus known to be associated with infection neutralization. The adrl23 shows an "L" shaped helix-turn-helix topology with two β-turns formed by residues Ala^{130}-Asp^{133} and Asp^{133}-Val^{136} intervening the N- and C-terminal helices. The N-terminal α-helix consists of residues Ser^{124}-Gln^{129} whereas the C-terminal 3_{10} helix is formed by residues Val^{136}-Tyr^{140}. The β-turns overlap partially with the putative "conformational" epitope. The overall topology of adrl23 is primarily maintained by hydrophobic interactions involving Phe^{127}, Leu^{131}, Leu^{132}, Val^{136}, and Tyr^{140} that are clustered on one side of the molecule. An additional hydrophobic stabilization comes from Phe^{141} that is buried inside the concave side of the molecule. A network of hydrogen bonds formed among Thr^{125}, His^{128}, and Arg^{137} further contribute to the "boomerang-shaped" architecture of adrl23. The N-terminus of adrl23 is immobile due to a hydrogen bond between the N-terminal amide proton of Asn^{123} and the hydroxyl oxygen of Thr^{126}. The side chains of Asp^{133}, Arg^{135}, Val^{136}, Leu^{139}, and Tyr^{140} that were shown to be important for binding to a monoclonal antibody H8 mAb are surface exposed.

Keywords: Hepatitis B virus; Surface antigen; PreS2; Monoclonal antibody; NMR

1. Introduction

Hepatitis B is a major disease affecting more than 300 million people worldwide and is a particularly serious health threat in Asia and the third-world countries (Blumberg and London, 1982; Stephenne, 1990). Hepatitis B virus (HBV) is a prototype of the family of Hepadnaviridae (Chisari et al., 1989) and the symptom of HBV infection is highly polymorphic ranging from asymtomatic infection to acute hepatitis and chronic liver diseases (Dreesman et al., 1982; Ganem and Varmus, 1987). Prolonged hepatitis B infection often develops into cirrhosis and hepatocellular carcinoma (Beasley et al., 1981). During HBV infection, two forms of particles, a 22-nm spherical or filamentous particle and a 42-nm virion or Dane particle, circulate in the serum of the HBV carriers. Each of these particles possesses the hepatitis B surface antigen (HBsAg) on its surface, the known classical marker for chronic infection by HBV (Alexander et al., 1984; Dubois et al., 1980). The entire HBsAg is composed of three proteins that are derived from three or four open reading frames (ORFs) of the HBV surface gene (Heerman et al., 1984). The first is the major S protein (designated as SI-226) which is encoded by the *S* gene and exists in two forms, one with a single glycosylation at Asn^{146} (gp27) and the other with no glycosylation. The second, called middle or M protein, is composed of the S protein plus a 55 amino acid N-terminal extension called preS2. This protein exists as two glycosylated forms, gp33 and gp36 with Asn^{123} being 100% glycosylated in both forms. Finally, the third protein is termed large or L protein and is encoded by *preS1*, *preS2* and the *S* gene of the HBV (Heerman et al., 1984; Stibbe and Gerlich, 1983). This protein is also present either in a single glycosylated form (gp42) or in a

Abbreviations: HBV, hepatitis B virus; mAb, monoclonal antibody; NMR, nuclear magnetic resonance; RMSD, root mean square deviation; COSY, shift correlation spectroscopy; TOCSY, total COSY; NOESY, nuclear Overhauser enhancement spectroscopy; CSI, chemical shift index

* Corresponding author. Tel.: +82 42 860 4250; fax: +82 42 860 4259.
E-mail address: khhan600@kribb.re.kr (K.-H. Han).

0166-3542/$ – see front matter © 2006 Published by Elsevier B.V.
doi:10.1016/j.antiviral.2006.06.009

non-glycosylated form (p39). The amino acid sequences of *adr*, *ayw*, and *adw2* serotypes are homologous even though the preS1 region of the *ayw* serotype is 108 amino acids long whereas that in the *adr* serotype has 119 amino acids (Heerman et al., 1984).

The preS2 antigen exists in relatively low abundance in the sera of HBV but was shown to be highly immunogenic both to B and T cells (Milich et al., 1985; Milich, 1987) and is capable of binding to several human and animal anti-HBV antibodies (Neurath et al., 1986a). It also binds to human and chimpanzee albumin treated with glutaraldehyde (Itoh et al., 1992; Pontisso et al., 1989; Sobotta et al., 2000) and contains an epitope that elicits protective immunity in experimentally challenged chimpanzees (Itoh et al., 1986; Neurath et al., 1987a). A recent study has established an interesting correlation between naturally occurring deletions in preS2 region and hepatocellular carcinoma (Tai et al., 2002). A preS2 fragment (residues 120–145 when named from the N-terminus of L protein) is the most effective immunogen for production of antisera (Neurath et al., 1986a) and was proposed to contain a conformational epitope that would be important for infection neutralization (Neurath et al., 1986b; Lee et al., 1997). A 23-residue fragment of the preS2 region from the *adr* serotype HBV, named adrl23, with a sequence of NSTTFHQALLDPRVRGLYFPAGG (residues 123–145) forms a highly helical structure under hydrophobic solvents, some features of which appeared to be closely associated in an unexplained fashion with its binding to an *adr* serotype specific monoclonal antibody (H8 mAb) (Lee et al., 1994). Even though there are ample data dealing with functional aspects of both preS1 and preS2 proteins of HBV there is a paucity of structural information on these surface antigens (Lee et al., 1994; Saul et al., 1996; Maeng et al., 2001). Useful insights into the initial HBV infection step of hepatocytes can be gained by first understanding protein–protein or protein–antibody interactions associated with these surface antigens of HBV. Here, we describe the high-resolution solution structure of the major B cell epitopic domain in the preS2 from *adr* serotype HBV determined by ^{1}H two-dimensional nuclear magnetic resonance (NMR) methods and restrained molecular dynamics calculation. Results provide useful explanations for its binding profile to an *adr* serotype specific monoclonal antibody.

2. Materials and methods

2.1. Peptide preparation

Peptide synthesis was performed by the standard solid phase method using Fmoc as the Nα-amino protecting group. The peptide was purified by HPLC on a reverse phase C18 column (>95%) and its integrity was confirmed by a mass spectral analysis.

2.2. NMR experiments

Samples for the NMR studies were prepared in 95% CD_3OH/5% H_2O or in 100% D_2O with a final concentration of approximately 5 mM at pH 3.85. The pH was measured as a direct reading from a combination microelectrode calibrated at two reference pHs. All NMR experiments were performed using a Varian UNITY 500 spectrometer at two temperatures, 15 °C and 25 °C, in order to obtain unambiguous resonance assignment. Solvent suppression was carried out using selective, low-power (approximately 60 Hz field strength) irradiation of the water resonance during the relaxation delay of 1.5 s. Solvent suppression was also applied during the mixing period in the case of the NOESY or ROESY experiments. Mixing times of 80–300 ms for NOESY and ROESY were used. For TOCSY experiments, mixing times of 57–82 ms were applied.

In addition, the coupling constants for the backbone torsion angle were measured from phase-sensitive DQF-COSY experiments. In order to obtain $^3J_{\alpha\beta}$ coupling constants for χ^1 torsion angles the P.E. COSY experiment was performed in 100% D_2O. Spectral widths were 5 kHz in both dimensions. Typical 2D data 2048 complex points in t_2 dimension with 512 complex t_1 increments except for the DQF-COSY and P.E. COSY experiments where these numbers were doubled to give a final digital resolution of 1.2 Hz in the F2 dimension after a zero-filling. In order to monitor the H–D exchange of labile protons such as backbone amide protons and side chain amide protons a series of ^{1}H spectra were obtained after the fully protonated protein was dissolved in 100% D_2O.

2.3. Structure calculations

lnterproton distance restraints were derived primarily from NOESY spectra recorded with a mixing time of 150 ms obtained at 15 °C and were supplemented with 80 ms and 300 ms mixing times. The FELIX program in the NMR Refine module of Biosym 95.0 software (Molecular Simulation, Inc., San Diego, CA) was used for quantification of the NOE cross peak volumes and for converting them into upper bounds of interproton distances similar to the published procedure (Davis et al., 1993). As a distance reference, the NOE volumes of five non-overlapping geminal β-proton cross peaks were averaged and correlated with the appropriate geminal distance of 1.8 Å. Volume integration errors and influence of possible conformational averaging were taken into consideration by adding 0.5 Å and 1.0 Å to distance restraints involving only backbone protons and to those containing at least one side chain proton, respectively. In addition to the interproton distance restraints, dihedral angle restraints were derived from $^3J_{\mathrm{HNH}\alpha}$ coupling constants, with centered on $-120°$ ($\pm 30°$) for $^3J_{\mathrm{HNH}\alpha} > 8$ Hz and $-60°$ ($\pm 30°$) for $^3J_{\mathrm{HNH}\alpha} < 6$ Hz. The χ^1 torsion angle restraints were also obtained from $^3J_{\alpha\beta}$ coupling constants in combination with the $d_{\mathrm{N}\beta}$.

The 50 low-resolution structures were generated using DGII calculation based on the metric matrix (Molecular Simulation, Inc.). Automatic pseudo-atom constraint corrections and floating chirality for non-stereospecifically assigned protons are implemented in DGII. In order to refine the initial distance restraints and to obtain more accurate distance restraints, BKCALC (Banks et al., 1989) was run for the structures generated by DGII. The final restraint set included a total of 298 distance restraints which consisted of 133 intraresidue distances, 87 sequential, 52 medium range ($|i-j|<4$) and 26 long range

($|i-j| \geq 4$) inter-residue distances. Also included in the restraint file were 14 ϕ backbone dihedral angles restraints derived from $^3J_{HNH\alpha}$ and 11 χ^1 side chain torsion angle restraints derived from $^3J_{\alpha\beta}$. Next, the DGII-generated structures were refined by restrained molecular dynamics (Clore et al., 1987). The dynamics run lasted for 52 ps at 1000 K and 25 ps of annealing period down to 100 K, finally followed by a short energy minimization using a conjugate gradient method. The force constants for the *NOE* interproton distances and the torsion angle restraints were all set to 30.0 kcal/mol / Å^2. The atomic coordinates of adrl23 have been deposited in the Protein Data Bank (accession code 1WZ4).

3. Results

3.1. NMR spectroscopy and structure determination

Complete ^{1}H resonance assignment for the adrl23 was achieved by a combined use of DQF-COSY, TOCSY, and NOESY/ROESY followed by a sequential resonance assignment procedure (Billeter et al., 1982). Initial assignment of the spin systems to individual amino acids was done along the amide NH resonances. At this point unambiguous assignment of several amino acids such as His^{128}, Arg^{135}, and Arg^{137} were already possible by taking the advantage of their back-transfer cross peaks. Once the individual spin systems were classified according to the characteristic spin systems, sequential NOE cross peaks were used to finalize the assignment procedure. At 15 °C, all of the sequential $d_{\alpha N}$ type cross peaks were clearly visible allowing sequential resonance assignment. Data obtained at 25 °C were used in completing the resonance assignment for residues, His^{128}, Arg^{135}, and Arg^{137}. Fig. 1 shows the amide-aliphatic region of a NOESY spectrum obtained with a mixing time of 150 ms. Fig. 2 is the summary of sequential and medium range NOEs used for resonance assignment along with $^3J_{HNH\alpha}$. Small minor cross peaks (approximately 10% of the major cross peaks) were present in the spectra, which seem to originate from a *cis*-isomer due to the two prolines (Pro^{134} and Pro^{142}) in the peptide. Resonance assignment and subsequent structure calculations we report here are for the major form (*trans*-isomer) of adrl23 where all the prolines show sequential $d_{\alpha\delta}$ type cross peaks in the NOESY spectrum.

In addition to NOE-derived interproton distances, a total of 23 $^3J_{HNH\alpha}$ coupling constants for the backbone torsion angles were obtained from phase-sensitive DQF-COSY experiments. In addition, a P.E. COSY experiment was performed in 100% D_2O in order to obtain $^3J_{\alpha\beta}$ coupling constants for χ^1 torsion angles. A total of 11 χ^1 torsion angles were obtained from the measured $^3J_{\alpha\beta}$ values in conjunction with the $d_{N\beta}$. Some slowly exchanging protons were observable even at 400 min after the

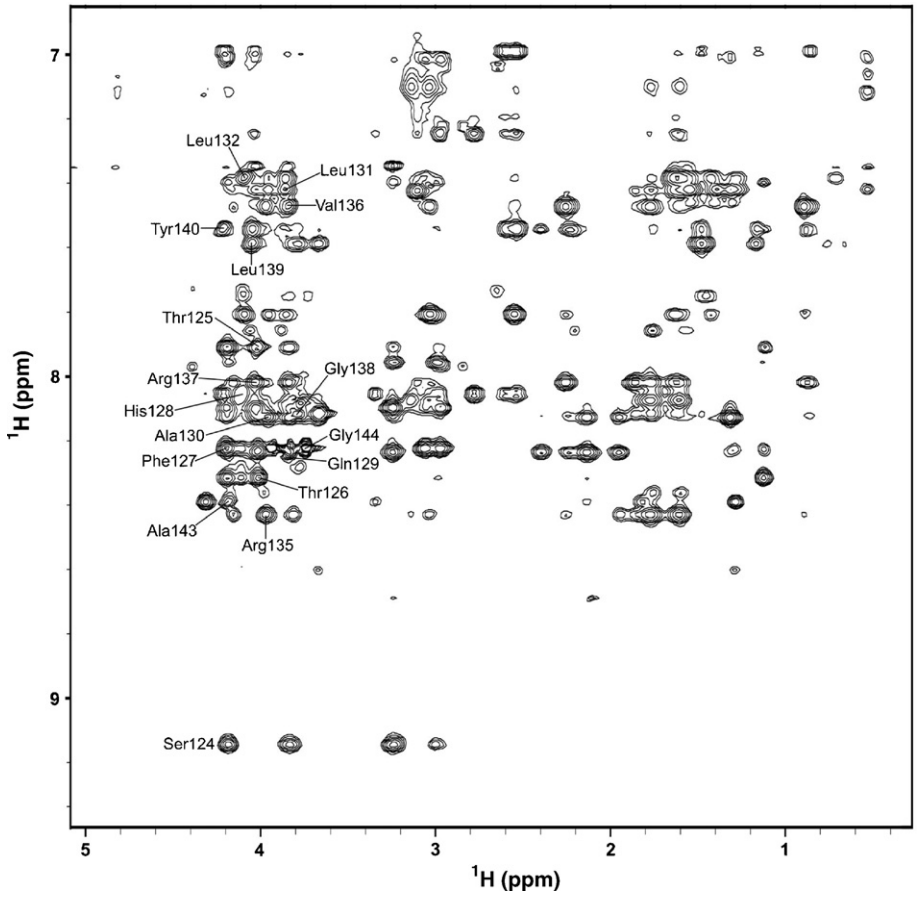

Fig. 1. A fingerprint region of a NOESY spectrum for adrl23 obtained at 15 °C. The sample is made up of 5 mM peptide 95% CD_3OH and 5% H_2O at pH 3.9. Assigned amino acid residues are labeled.

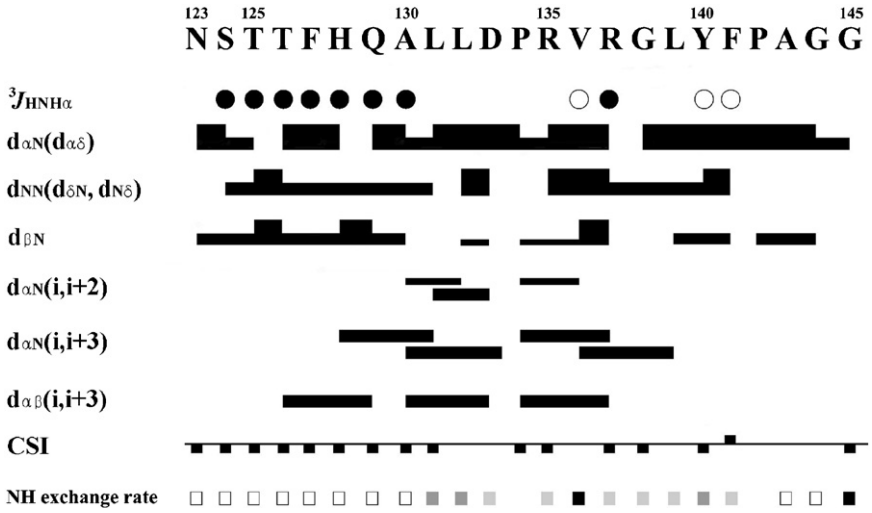

Fig. 2. A summary of short- and medium-range NOEs, $^3J_{HNH\alpha}$, and H_α proton chemical shift index (CSI) for adrl23. Thickness of bar represents relative strength (strong, medium, and weak) of NOEs. Filled circles are drawn when $^3J_{HNH\alpha} < 6$ Hz and open circles when $^3J_{HNH\alpha} > 8$ Hz. The filled squares above and below the horizontal line represent CSI values of +1 and −1, respectively. At the bottom shown are the exchange rates of NH protons when the peptide is dissolved in 100% D_2O. The white squares indicate the disappearance of NH proton signals within 78 min after deutration and the black squares indicate the existence of NH proton signals in 490 min after deutration. The squares are colored with a spectrum in which white to black represents fast to slow exchange rates, respectively.

addition of 100% D_2O as shown in Fig. 2. A summary of the distribution of the NOE restraints as a function of residue number is shown in Fig. 3A. Structure determination statistics are summarized in Table 1 and Fig. 3B–E. The structure of adrl23 is well-defined as reflected in the backbone and heavy atom root mean square deviations (RMSDs) of the final structures (over residues 2–21) that are 0.52 (±0.15) Å and 1.11 (±0.19) Å, respectively. All the backbone conformations are well defined except for the two C-terminal glycines. A unique result is that the N-terminus of adrl23 is quite immobile (see following sections).

Table 1
NMR structural determination statistics of adrl23 for an ensemble of 20 structures

Number of NOE distance restraints	298
Intraresidue	133
Sequential	87
Medium range (<4)	52
Long range (≥4)	26
Number of backbone dihedral angle restraints	14
Number of χ^1 torsional angle	11
Ramachandran plot regions (%)[a]	
Residues in most favored region	55.6
Residues in additional allowed region	43.2
Residues in generously allowed region	1.2
Residues in disallowed region	0.0
Angular order parameters (residues 2–21)[b]	
ϕ	0.996 ± 0.004
ψ	0.986 ± 0.026
χ^1	0.895 ± 0.198
RMSDs from NOE distance restraints (Å)	0.107 ± 0.003
RMSDs from the average structure (residues 2–21)	
Backbone atoms[c] (Å)	0.52 ± 0.15
Heavy atoms (Å)	1.11 ± 0.19

[a] The values are obtained by PROCHECK analysis (Laskowski et al., 1996).
[b] Values where applicable are the means ± standard deviations.
[c] C^a, $C > C^\alpha$, C'.

3.2. Description of the three-dimensional structure

A stereoview of the 20 final converged structures of adrl23 is shown in Fig. 4A. The adrl23, albeit a short peptide, forms a highly ordered structure under a hydrophobic condition used. The overall conformation of adrl23 is a helix-turn-helix, similar to that of melittin in a structural sense. A prominent feature of adrl23 is presence of two amphipathic helices that are intervened by two β-turns in the middle of the molecule near Pro^{134} (Fig. 4B). The helical nature of adrl23 was noted in previous CD studies that used hydrophobic solvents. In Fig. 2 presence of two helices in adrl23 is well supported by strong sequential d_{NN} as well as $d_{\alpha N(i,i+3)}$ type NOE cross peaks. In addition, chemical shift indices (CSI) (Wishart et al., 1992) of α-protons and the small $^3J_{HNH\alpha}$ values of less than 6 Hz point to location of the helices. This observation is consistent with a theoretical prediction made by STRIDE (Frishman and Argos, 1995).

The first helix at the N-terminus of adrl23 is a highly stable α-helix and consists of residues Ser^{124}-Gln^{129} while the second at the C-terminus is a somewhat loose 3_{10} helix formed by residues Val^{136}-Tyr^{140}. Two type IV β-turns are found at residues Ala^{130}-Asp^{133} and Asp^{133}-Val^{136}, respectively. These turns are able to form because specific backbone torsion angles of Asp^{133} and Pro^{135} are allowed due to the hydrogen bond between the guanidyl group of Arg^{137} and the imidazole ring $N_\delta H$ proton in His^{128}. Presence of this hydrogen bond is reflected in the slow H–D exchange rate of the guanidyl NH protons in Arg^{137} (data not shown). Formation of two stable turns in the middle of adrl23 is also augmented by the intramolecular hydrophobic interactions among the side chains of Leu^{131}, Leu^{132}, and Val^{136}. An extremely slow H–D exchange rate of the backbone amide proton of Val^{136} (Fig. 2) is due to a hydrogen bond between the

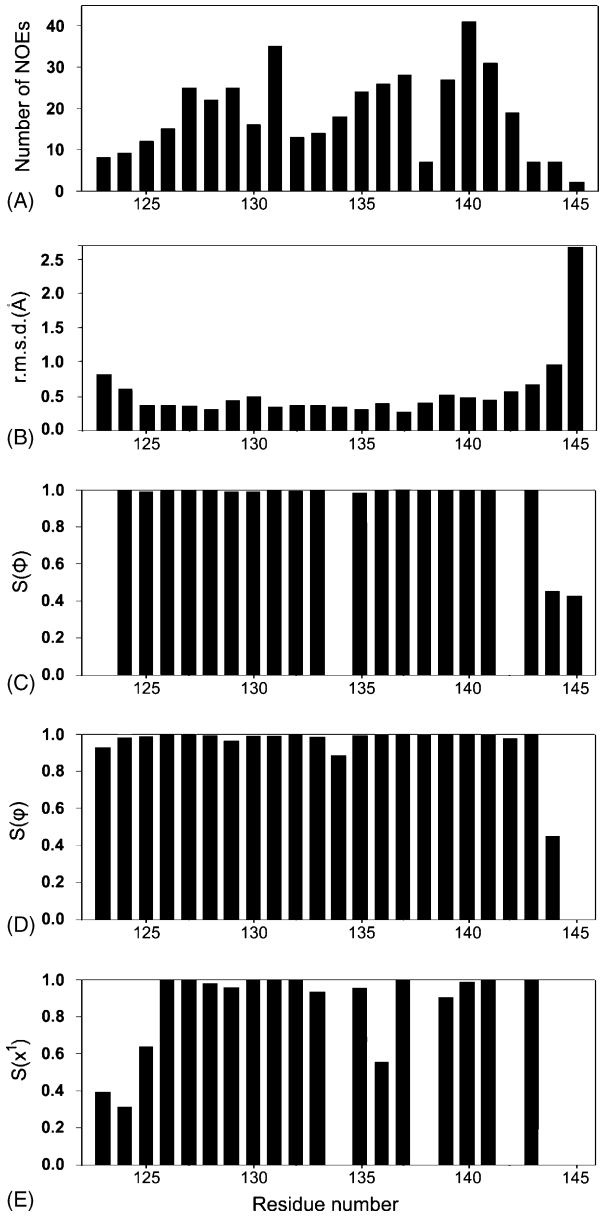

Fig. 3. NMR statistics of adrl23 for an ensemble of 20 structures. Plots as a function of the residue number of (A) the number of NOE constraints used in the structure refinement, (B) the average RMSD for the backbone heavy atoms, and (C–E) the angular order parameters for the backbone and first side chain dihedral angles.

backbone amide proton of Val^{136} and the carbonyl oxygen of Asp^{133}. A similarly slow exchange rate is observed for the backbone amide proton of Gly^{145} as this proton forms a hydrogen bond with its own carboxylate moiety and the carbonyl oxygen of Gly^{144}. Such an overall disposition of two helices connected by two turns exposes the side chains of Asp^{133}, Arg^{135}, Val^{136}, Leu^{139}, and Tyr^{140}, which may interact with target molecules.

The surface representation of adrl23 described in Fig. 5 shows that the molecule is amphipathic. The adrl23 resembles a "boomerang" whose large top side (front side in Fig. 5A) is covered with several hydrophobic residues (Phe^{127}, Leu^{131}, Leu^{132}, Val^{136}, Leu^{139}, and Tyr^{140}) and the other side with two hydrophilic residues (Asp^{133} and Arg^{135}). The benzene ring of Phe^{141} is mostly buried in the concave side and makes hydrophobic contacts with the methylene groups of His^{128} and Arg^{137}. The isopropyl group of Val^{136} is also partially buried (located behind Leu^{132} in Fig. 4B). An atypical structural feature in adrl23 is its immobile N-terminus (Fig. 4) unlike typically disordered termini of proteins or peptides in solution. Such a rigidity is conferred by a hydrogen bond between the N-terminal amide proton of Asn^{123} and the hydroxyl group of the Thr^{126}. Deep down in the molecular core of adrl23 lie a network of hydrogen bonds formed among the hydroxyl group of Thr^{125}, the imidazol ring $N_{\delta}H$ of His^{128}, and the guanidyl group of Arg^{137}. This hydrogen bonded hydrophilic core is concealed underneath a large hydrophobic surface created by Phe^{127}, Leu^{131}, and Phe^{141}.

4. Discussion

Even though the full preS2 region of HBV is composed of 55 residues, earlier works demonstrated that only its N-terminal domain near residues 120–145 is particularly immunogenic and infection-neutralizing (Neurath et al., 1986a; Neurath et al., 1987b). In a more recent competitive ELISA study it was shown that binding of a full preS2 to an *adr* serotype specific H8 mAb could be inhibited by various preS2 peptides, among which adrl23 exhibited the highest inhibitory activity (Lee et al., 1994). The adrl23 peptide studied here, being a short peptide, is not much structured in water, but becomes ordered in hydrophobic solvents (Lee et al., 1994). NMR structural studies of proteins and peptides are typically carried out at slightly acidic conditions (pH 3–6), which enable one to better observe the resonances from labile protons such as backbone amide NHs by minimizing their exchange rates (Wüthrich, 1986). The structures of peptides including that of adrl23 determined under such conditions are well known to be invariant regardless of pH (Wüthrich, 1995). Hydrophobic solvents are often used as they are believed to reasonably mimic the hydrophobic ligand-binding pocket in target proteins. Bulky aromatic hydrophobic residues such as Trp, Tyr, and Phe are often found in the antigen binding pocket of antibodies (Davies and Cohen, 1996; Padlan, 1994; Stites, 1997). Many short antigenic peptides have in fact been found to undergo a structural transition from an unstructured state into a β-turn (Nair et al., 2002) or an α-helix upon binding to an antibody (Stanfield and Wilson, 1995; Tsang et al., 1992). When a preS2 fragment (residues 134–140) is inserted into maltodextrin binding protein, its residues 134–140 form a two-turn helix, one turn of which is an α-helix and the other is a 3_{10} helix (Saul et al., 1996). This two-turn helix is very similar to the C-terminal two-turn 3_{10} helix present in the adr123 structure described here.

Extensive mutation studies on adr123 have been carried out and shown that binding of adrl23 to H8 mAb is governed mainly by residues Phe^{127}, Leu^{131}, Asp^{133}, Val^{136}, Arg^{137}, Tyr^{140}, and Phe^{141} (Lee et al., 1996; Lee et al., 1997). Yet no succinct explanation was given how the binding is controlled by these residues. The reduced antibody binding may arise from removal of direct antibody contacts or could be due to structural disruption that misplaces residues that otherwise would contact H8 mAb. A fragment of adrl23 (residues 130–145) that con-

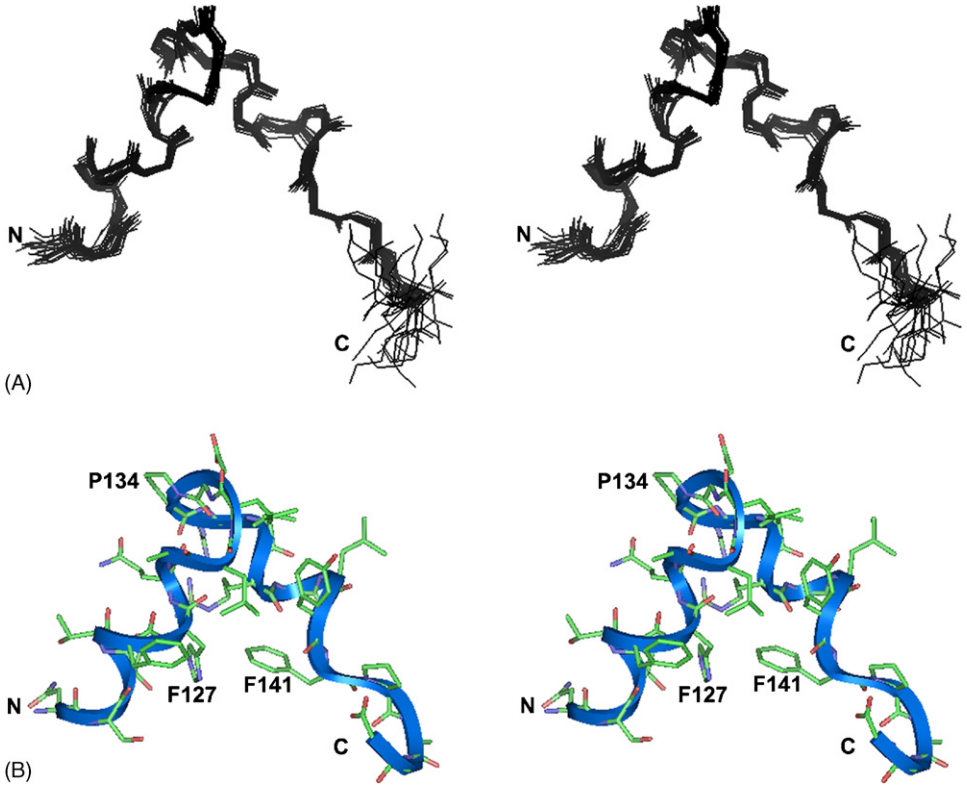

Fig. 4. A stereoview of the final 20 structures for adrl23. (A) Backbone superposition of the 20 converged structures of adrl23. The N- and C-terminus are labeled with capital letters N and C, respectively. (B) Ribbon diagram of a representative structure of adrl23. The ribbon traces the molecular backbone and selected residues are labeled.

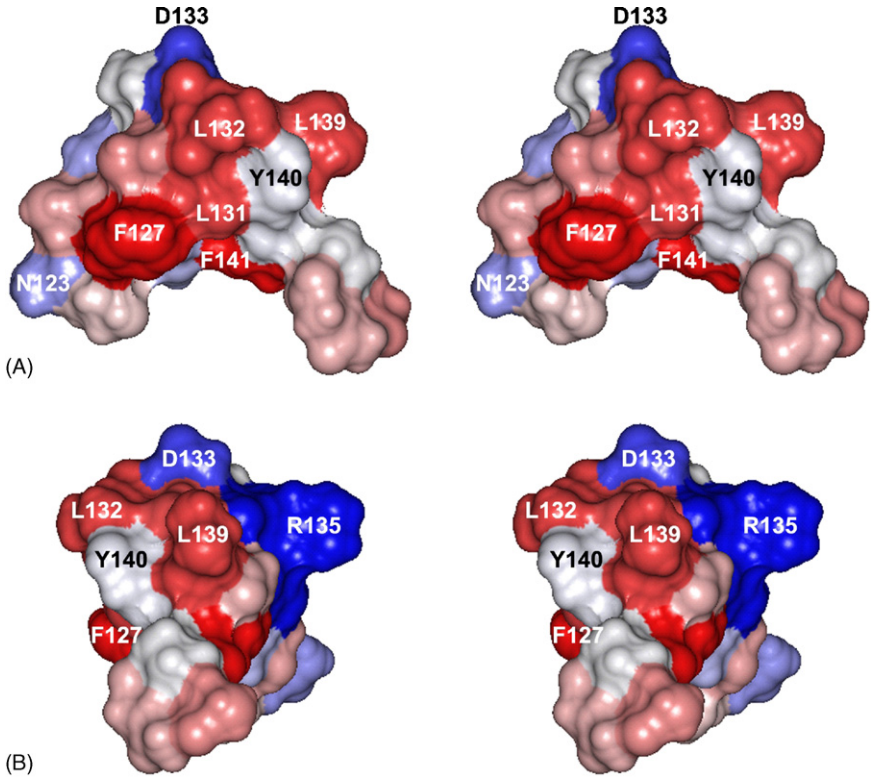

Fig. 5. Connolly surface representation of adrl23. The stereoviews of Connolly surface (Connolly, 1983) on adrl23 are shown with the hydropathy property with a color spectrum in which red to blue stands for hydrophobic to charged, respectively. Note the amphipathic distribution of residues in the adrl23 surface. (A) The view is the same as that of Fig. 4B. (B) The 90° rotated view from (A) in *y*-axis.

tains the putative conformational epitope does not bind H8 mAb (Lee et al., 1994; Lee et al., 1997), suggesting that the whole adrl23 is required to bind to the antibody. The structure of adrl23 presented here provides reasonable explanations for such observations. For example, adrl23 structure predicts that replacing any of four residues (Phe^{127}, Leu^{131}, Arg^{137}, and Phe^{141}) should significantly disrupt antibody binding as these residues are critical for maintenance of the overall architecture of adrl23. And, that is precisely what has been observed (Lee et al., 1996; Lee et al., 1997). In addition, the structure suggests that unless Asp^{133}, Val^{136}, and Tyr^{140} make direct contacts with H8 mAb mutating any of these residues would not affect antibody binding as they are not critically involved in maintaining the overall structure of adrl23. Any single mutation of these residues was shown to completely abolish (<5%) binding of adrl23 to H8 mAb, strongly arguing that they must be direct contact residues to H8 mAb. Interestingly, Arg^{135} and Leu^{139} did not influence the binding of adrl23 to H8 mAb at all (Lee et al., 1996) even though their side chains are prominently surface exposed. Thus, these two residues neither are likely to be direct antibody contacting residues nor to serve as "structural maintenance" residues. One cannot exclude the possibility that, being surface exposed, they might be important for binding to another antibody. These results are consistent with the claim that the putative conformational B cell epitope consists of residues 130–145 (Lee et al., 1997).

Both Phe^{127} and Leu^{131} are crucial for H8 mAb binding (Lee et al., 1996; Lee et al., 1997). These two residues stabilize the structure of adrl23 by strong hydrophobic interactions (Fig. 5), in particular, the integrity of the N-terminal α-helix and the first β-turn. However, as both residues are surface exposed as well it is not clear how, due to loss of direct antibody contacts or because of structural disruption, antibody binding becomes reduced (<3%) upon mutating either of these residues. It was postulated that binding of adrl23 to H8 mAb is closely associated with the structural integrity of the N-terminal helix based upon the fact that mutations that strengthen the helicity of this helix increase the affinity of adrl23 to H8 mAb while those that lower the helicity weaken the binding with H8 mAb (Lee et al., 1994). For example, mutating Thr^{125} by a glutamate was shown to increase the affinity. In the structure of adrl23 one finds that the side chain carboxylate of a glutamate would make a stronger hydrogen bond to the imidazole group of His^{128} than a hydroxyl group of a threonine, enhancing the stability of the N-terminal helix. Likewise, replacing His^{128} with a glutamate would favor binding of adrl23 to H8 mAb as the guanidino group of Arg^{137} would form stronger hydrogen bonds with the side chain carboxylate of a glutamate than with the imidazole moiety of His^{128}, which ends up stabilizing both the N-terminal helix and the overall structure of adrl23. Introducing a positively charged residue such as a lysine into the N-terminal helix greatly reduced antibody binding (Lee et al., 1994). The adrl23 structure predicts that such a mutation would not only break hydrogen bonding but also place steric hindrance that severely disturb the overall topology of adrl23.

Our structure of adrl23 also suggests that the observed differences in H8 mAb binding among different serotypes be related to conformational differences of various preS2 peptides. The adrl23 analog fragment in an *ayw* serotype preS2 (aywl23 hereafter) and that in an *adw2* serotype preS2 (adw2–123 hereafter) binds to H8 mAb with a reduced affinity (−34% of adrl23) and exhibits no binding, respectively (Lee et al., 1994). The amino acid sequence of ayw123 differs only in two positions ($Ala^{130} \rightarrow Thr^{130}$ and $Leu^{132} \rightarrow Gln^{132}$) from that of adrl23. These substitutions must disturb the turn region to some extent. However, since neither of these residues are so much structurally crucial as the other residues mentioned above ayw123 should still be able to bind H8 mAb, albeit with a reduced affinity as was shown (Lee et al., 1994). On the other hand, the corresponding preS2 domain in *adw*2 serotype (adw2–123 hereafter) has four residues ($Thr^{126} \rightarrow Ala^{126}$, $Ala^{130} \rightarrow Thr^{130}$, $Leu^{132} \rightarrow Gln^{132}$, and $Phe^{141} \rightarrow Leu^{141}$) that differ from adrl23. Replacing Thr^{126} in adrl23 by an alanine may mobilize the N-terminus of the peptide since the hydroxyl group of Thr^{126} forms a hydrogen bond with the N-terminal amide proton. Otherwise, substitution at this position would not significantly disrupt the structure as Thr^{126} is facing outside and is not a part of the conformational epitope, which is located beyond Phe^{127} (Lee et al., 1997; Neurath et al., 1986b). The $Phe^{141} \rightarrow Leu^{141}$ substitution, unlike the $Thr^{126} \rightarrow Ala^{126}$, is likely to significantly disturb the hydrophobic core of adrl23 at the concave side as a leucine may not be as effective as a phenylalanine in making hydrophobic interactions. There is also a possibility that the $Phe^{141} \rightarrow Leu^{141}$ substitution might nullify potential π-cation interactions between the benzene ring and the imidazole group of His^{128} or the guanidyl group of Arg^{137}. Thus, combined effects of $Phe^{141} \rightarrow Leu^{141}$ substitution on top of $Ala^{130} \rightarrow$

Thr^{130} and $Leu^{132} \rightarrow Gln^{132}$ replacements along with the increased mobility at the N-terminus of adrl23 must be sufficient to abolish its ability to bind H8 mAb. Preliminary NMR studies, secondary structure prediction and CD results on ayw123 and adw2–123 indicate that their structures are indeed different from that of adrl23, the former slightly and the latter significantly (K. Han, unpublished results). The Asn^{123} in the M protein is always N-glycosylated in nature. Such a modification may mobilize the N-terminus of adrl23 since the hydrogen bonding between Asn^{123} and Thr^{126} could be sterically hampered. Nevertheless, it is unlikely that the glycosylation at Asn^{123} affects binding of H8 mAb to adrl23 since the actual antibody contacts appear to be located near the turn regions in adrl23.

Despite continued efforts to unambiguously identify a hepatocyte receptor for HBV (De Falco et al., 2001; Neurath et al., 1992; Ryu et al., 2000), it is not clear whether one of the reported proteins may represent a true hepatocyte receptor. While HBV vaccines are available and successful for the most part there is still a problem associated with non-responding individuals. Anti-HBV drugs based on polymerase inhibition are also commercially available (Jilg, 1998; Mahoney and Kane, 1999; West et al., 1990) yet one has to cope with development of drug resistance after a long-term use. One may use a strategy of blocking viral attachment to hepatocytes at an early stage of infection as has been demonstrated in the case of human immunodeficiency virus-1 against which a peptide inhibitor "Pentafuside" has been developed (Chan and Kim, 1998). It remains to be seen if adrl23 can be applied against HBV infection as Pentafuside since both

adrl23 and the N-terminal domain of preS2 (residues 120–145) are highly immunogenic and infection-neutralizing (Lee et al., 1994; Neurath et al., 1986a, 1987b).

Acknowledgements

The present work has been supported by a grant NBM0900513 to K.H. from Molecular & Cellular BioDiscovery Research Group and the Ministry of Science and Technology of Korea.

References

Alexander, J.J., Patzer, E., Nakamura, G., Yaffe, A., 1984. Intracellular transport and secretion of hepatitis B surface antigen in mammalian cells. J. Virol. 51, 346–353.

Banks, K.M., Hare, D.R., Reid, B.R., 1989. Three-dimensional solution structure of a DNA duplex containing the Bell restriction sequence: two-dimensional NMR studies, distance geometry calculations, and refinement by back-calculation of the NOESY spectrum. Biochemistry 28, 6996–7010.

Beasley, R.P., Hwang, L.-Y., Lin, C.C., Chien, C.S., 1981. Hepatitis B immune globulin (HBIG) efficacy in the interruption of perinatal transmission of hepatitis B virus carrier state. Initial report of a randomised double-blind placebo-controlled trial. Lancet 2, 1129–1133.

Billeter, M., Braun, W., Wuthrich, K., 1982. Sequential resonance assignments in protein ^{1}H nuclear magnetic resonance spectra. Computation of sterically allowed proton–proton distances and statistical analysis of proton–proton distances in single crystal protein conformations. J. Mol. Biol. 155, 321–346.

Blumberg, B.S., London, T., 1982. Hepatitis B virus: pathogenesis and prevention of primary cancer of the liver. Cancer 50, 2657–2665.

Chan, D.C., Kim, P.S., 1998. HIV entry and its inhibition. Cell 93, 681–684.

Chisari, F.V., Ferrari, C., Mondelli, M., 1989. Hepatitis B virus structure and biology. Microb. Pathog. 6, 311–325.

Clore, G.M., Sukumaran, D.K., Nilges, M., Gronenborn, A.M., 1987. The three-dimensional structure of phoratoxin in solution: combined use of nuclear magnetic resonance, distance geometry and restrained molecular dynamics. Biochemistry 26, 1732–1745.

Connolly, M.L., 1983. Solvent-accessible surfaces of proteins and nucleic acids. Science 221, 709–713.

Davies, D.R., Cohen, G.H., 1996. Interactions of protein antigens with antibodies. Proc. Natl. Acad. Sci. U.S.A. 93, 7–12.

Davis, J.H., Bradley, E.K., Miljanich, G.P., Nadasdi, L., Ramachandran, J., Basus, V.J., 1993. Solution structure of omega-conotoxin GVIA using 2-D NMR spectroscopy and relaxation matrix analysis. Biochemistry 32, 7396–7405.

De Falco, S., Ruvoletto, M.G., Verdoliva, A., Ruvo, M., Raucci, A., Marino, M., Senatore, S., Cassani, G., Alberti, A., Pontisso, P., Fassina, G., 2001. Cloning and expression of a novel hepatitis B virus-binding protein from HepG2 cells. J. Biol. Chem. 276, 36613–36623.

Dreesman, G.R., Sanchez, Y., Ionescu-Matiu, L., Sparrow, J.T., Six, H.R., Peterson, D.L., Hollinger, F.B., Melnick, J.L., 1982. Antibody to hepatitis B surface antigen after a single inoculation of uncoupled synthetic HBsAg peptides. Nature 295, 158–160.

Dubois, M.-F., Pourcel, C., Rousset, S., Chany, C., Tiollais, P., 1980. Excretion of hepatitis B surface antigen particles from mouse cells transformed with cloned viral DNA. Proc. Natl. Acad. Sci. U.S.A. 77, 4549–4553.

Frishman, D., Argos, P., 1995. Knowledge-based protein secondary structure assignment. Proteins 23, 566–579.

Ganem, D., Varmus, H.E., 1987. The molecular biology of the hepatitis B viruses. Annu. Rev. Biochem. 56, 651–693.

Heerman, K.H., Goldmann, U., Schwartz, W., Seyffarth, T., Baumgarten, H., Gerlich, W., 1984. Large surface proteins of hepatitis B virus containing the pre-S sequence. J. Virol. 52, 396–402.

Itoh, Y., Takai, E., Ohuma, H., Kitajima, K., Tsuda, F., Machida, A., Mishiro, S., Nakamura, T., Miyakawa, Y., Mayumi, M., 1986. A synthetic peptide vaccine involving the product of the pre-S(2) region of hepatitis B virus DNA: protective efficacy in chimpanzees. Proc. Natl. Acad. Sci. U.S.A. 84, 9174–9178.

Itoh, Y., Kuroda, S., Miyasaki, T., Otaka, S., Fujisawa, Y., 1992. Identification of polymerized-albumin receptor domain in the preS2 region of hepatitis B virus surface antigen M protein. J. Biotechnol. 23, 71–82.

Jilg, W., 1998. Novel hepatitis B vaccines. Vaccine 16, 65–68.

Laskowski, R.A., Rullman, J.A., MacArthur, M.W., Kaptein, R., Thornton, J.M., 1996. AQUA and PROCHECK-NMR: programs for checking the quality of protein structures solved by NMR. J. Biomol. NMR 8, 477–486.

Lee, M.K., Kim, K.L., Hahm, K.S., Yang, K.H., 1994. Structure–antigenicity relationship of peptides from the preS2 region of the hepatitis B virus surface antigen. Mol. Biol. Int. 34, 159–168.

Lee, M.K., Kim, K.L., Hahm, K.S., 1996. Epitope mapping of preS2 of the hepatitis B virus surface antigen against a conformation-dependent monoclonal antibody using synthetic peptides. Mol. Biol. Int. 40, 1077–1085.

Lee, M.K., Kim, K.L., Hahm, K.S., 1997. Evaluation of the N-terminal role in peptide antigenicity of the preS2 region of the hepatitis B virus surface antigen. Mol. Cells 7, 340–346.

Maeng, C.Y., Oh, M.S., Park, I.H., Hong, H.J., 2001. Purification and structural analysis of the hepatitis B virus preS1 expressed from *Escherichia coli*. Biochem. Biophys. Res. Commun. 282, 787–792.

Mahoney, F.J., Kane, M., 1999. In: Plotkins, S.A., Orenstein, W.A. (Eds.), Hepatitis B vaccine. Saunders, London, pp. 158–182.

Milich, D.R., Thornton, G.B., Neurath, A.R., Kent, S.B.H., Michel, M., Tiollais, P., Chisari, F.V., 1985. Enhanced immunogenicity of the pre-S region of hepatitis B surface antigen. Science 228, 1195–1199.

Milich, D.R., 1987. Genetic and molecular basis for T- and B-cell recognition of hepatitis B viral antigens. Immunol. Rev. 99, 71–103.

Nair, D.T., Singh, K., Siddiqui, Z., Nayak, B.P., Rao, K.V., Salunke, D.M., 2002. Epitope recognition by diverse antibodies suggests conformational convergence in an antibody response. J. Immunol. 168, 2371–2382.

Neurath, A.R., Kent, S.B., Parker, K., Prince, A.M., Strick, N., Brotman, B., Sproul, P., 1986a. Antibodies to a synthetic peptide form the PreS 120–145 region of the hepatitis B virus envelope are virus-neutralizing. Vaccine 4, 35–37.

Neurath, A.R., Adamowicz, P., Kent, S.B., Riottot, M.M., Strick, N., Parker, K., Offensperger, W., Petit, M.A., Wahl, S., Budkowska, A., Girard, M., Pillot, J., 1986b. Characterization of monoclonal antibodies specific for the pre-S2 region of the hepatitis B virus envelope protein. Mol. Immunol. 23, 991–997.

Neurath, A.R., Kent, S.B., Strick, N., Parker, K., Courouce, A.M., Riottot, M.M., Petit, M.A., Budkowska, A., Girard, M., Pillot, J., 1987a. Antibodies to synthetic peptides from the pre-S1 and pre-S2 regions of one subtype of the hepatitis B virus (HBV) envelope protein recognize all HBV subtypes. Mol. Immunol. 24, 975–980.

Neurath, A.R., Adamowicz, P., Riottot, M.M., Prince, P., Strick, N., Parker, K., Petit, M.A., Budkowska, A., Girard, M., 1987b. Immunological cross-reactivity between preS2 sequences of the hepatitis B virus envelope proteins corresponding to serological subtypes adw2 and ayw. Mol. Immunol. 24, 561–568.

Neurath, A.R., Strick, N., Sproul, P., 1992. Search for hepatitis B virus cell receptors reveals binding sites for interleukin 6 on the virus envelope protein. J. Exp. Med. 175, 461–469.

Padlan, E.A., 1994. Anatomy of the antibody molecule. Mol. Immunol. 31, 169–217.

Pontisso, P., Petit, M.-A., Bankowski, M.J., Peeples, M., 1989. Human liver plasma membranes contain receptors for the hepatitis B virus preS1 region and, via polymerized human serum albumin, for the preS2 region. J. Virol. 63, 1981–1988.

Ryu, C.J., Cho, D.Y., Gripon, P., Kim, H.S., Guguen-Guillouzo, C., Hong, H.J., 2000. An 80-kilodalton protein that binds to the pre-S1 domain of hepatitis B virus. J. Virol. 74, 110–116.

Saul, F.A., Normand, B.V., Lema, F., Bentley, G.A., 1996. Crystal structure of a recombinant form of the maltodextrin-binding protein carrying an inserted sequence of a B-cell epitope from the preS2 region of hepatitis B virus. Proteins 27, 1–8.

Sobotta, D., Sominskaya, I., Jansons, J., Meisel, H., Schmitt, S., Heermann, K.H., Kaluza, G., Pumpens, P., Gerlich, W.H., 2000. Mapping of immun-

odominant B-cell epitopes and the human serum albumin-binding site in natural hepatitis B virus surface antigen of defined genotypes. J. Gen. Virol. 81, 369–378.

Stanfield, R.L., Wilson, L.A., 1995. Protein–peptide interactions. Curr. Opin. Struct. Biol. 5, 103–113.

Stephenne, J., 1990. Development and production aspects of a recombinant yeast-derived hepatitis B vaccine. Vaccine 8 (Suppl.), S69–S73.

Stibbe, W., Gerlich, W.H., 1983. Structural relationships between minor and major proteins of hepatitis B surface antigen. J. Virol. 46, 626–628.

Stites, W.E., 1997. Protein–protein interactions: interface structure, binding thermodynamics, and mutational analysis. Chem. Rev. 97, 1233–1250.

Tai, P.C., Suk, P.C., Gerlich, W.H., Neurath, A.R., Shih, C., 2002. Hypermodification and immune escape of an internally deleted middle-envelope (M) protein of frequent and predominant hepatitis B virus variants. Virology 292, 44–58.

Tsang, P., Ranee, M., Fieser, T.M., Ostresh, J.M., Houghten, R.A., Lerner, R.A., Wright, P.E., 1992. Conformation and dynamics of an Fab′-bound peptide by isotope-edited NMR spectroscopy. Biochemistry 31, 3862–3871.

West, D.J., Calandra, G.B., Ellis, R.W., 1990. Vaccination of infants and children against hepatitis B. Pediatr. Clin. North Am. 37, 585–601.

Wishart, D.S., Sykes, B.D., Richards, F.M., 1992. The chemical shift index: a fast and simple method for the assignment of protein secondary structure through NMR spectroscopy. Biochemistry 31, 1647–1651.

Wüthrich, K., 1986. NMR of Proteins and Nucleic Acids. John Wiley and Sons, New York.

Wüthrich, K., 1995. NMR in Structural Biology. World Scientific, Singapore.